Epigenetics & Chromatin

RESEARCH Open Access

FOSL1 is a key regulator of a super-enhancer driving TCOF1 expression in triple-negative breast cancer

Qingling He[1†], Jianyang Hu[1,2†], Hao Huang[1], Tan Wu[1], Wenxiu Li[1], Saravanan Ramakrishnan[1], Yilin Pan[1], Kui Ming Chan[1,2], Liang Zhang[1,2], Mengsu Yang[1,2], Xin Wang[3] and Y. Rebecca Chin[1,2*]

Abstract

Triple-negative breast cancer (TNBC) is an aggressive subtype of breast cancer with an unmet clinical need, but its epigenetic regulation remains largely undefined. By performing multiomic profiling, we recently revealed distinct super-enhancer (SE) patterns in different subtypes of breast cancer and identified a number of TNBC-specific SEs that drive oncogene expression. One of these SEs, TCOF1 SE, was discovered to play an important oncogenic role in TNBC. However, the molecular mechanisms by which TCOF1 SE promotes the expression of the TCOF1 gene remain to be elucidated. Here, by using combinatorial approaches of DNA pull-down assay, bioinformatics analysis and functional studies, we identified FOSL1 as a key transcription factor that binds to TCOF1 SE and drives its overexpression. shRNA-mediated depletion of FOSL1 results in significant downregulation of TCOF1 mRNA and protein levels. Using a dual-luciferase reporter assay and ChIP-qPCR, we showed that binding of FOSL1 to TCOF1 SE promotes the transcription of TCOF1 in TNBC cells. Importantly, our data demonstrated that overexpression of FOSL1 drives the activation of TCOF1 SE. Lastly, depletion of FOSL1 inhibits tumor spheroid growth and stemness properties of TNBC cells. Taken together, these findings uncover the key epigenetic role of FOSL1 and highlight the potential of targeting the FOSL1-TCOF1 axis for TNBC treatment.

Keywords Transcription factor, Breast cancer, Super-enhancer, Gene regulation, FOSL1

Introduction

Breast cancer, the most commonly occurring cancer in women worldwide, is a heterogeneous disease with different biological and clinical outcomes [1]. Triple-negative breast cancer (TNBC) - an aggressive subtype of breast cancer where tumor cells are lack of the expression of estrogen receptors (ER), progesterone receptors (PR), and without overexpression of human epidermal growth factor receptor 2 (HER2) - accounts for up to 20% of all diagnosed breast cancer cases and with limited targeted therapeutics [2]. Currently, conventional chemotherapy, usually with high toxicity, is still the main clinical treatment option for patients with TNBC [3]. This underscores the importance of dissecting molecular

†Qingling He and Jianyang Hu contributed equally to this work.

*Correspondence:
Y. Rebecca Chin
rebecca.chin@cityu.edu.hk
[1]Tung Biomedical Sciences Centre, Department of Biomedical Sciences, City University of Hong Kong, Kowloon, Hong Kong, China
[2]City University of Hong Kong Shenzhen Research Institute, Shenzhen, China
[3]Department of Surgery, The Chinese University of Hong Kong, New Territories, Hong Kong, China

mechanisms driving TNBC tumorigenesis in order to discover new therapeutic targets for this malignant subtype.

Super-enhancers (SEs) are characterized by large clusters of neighbouring active enhancers, enriched with transcription factors (TFs), coactivators and mediators, that control gene expression programs. In addition to regulating key cell identity-related genes, SEs have been shown to drive oncogene expression in different types of cancer [4]. For example, SEs that drive MYC oncogene expression were found to be focally amplified in various carcinomas [5]. SEs preferentially amplified in ovarian cancer have also been identified and determined for their roles in tumor cell proliferation and migration via regulating oncogenic gene expression networks [6]. In our recent work, we uncovered that the heterogeneity of SEs in breast cancer subtypes, and identified several oncogenes, including FOXC1, MET, and ANLN, that are specifically regulated by TNBC-specific SEs [7]. Furthermore, we discovered TCOF1, one of the novel genes driven by TNBC-specific SEs, as a key regulator for TNBC tumor growth and stemness mediated by KIT [8].The upstream regulator of TCOF1, however, remains unknown. Although it has been widely reported that master TFs occupy and modulate SEs of cell type-determining genes, oncogenic TFs that bind to and regulate TNBC-specific SEs are poorly understood. In the present study, we set off to identify TFs which bind to TNBC-specific SE region of TCOF1 to drive its expression.

Fos-like antigen 1 (FOSL1; also known as FRA-1), a member of the FOS family proteins, dimerizes with JUN family proteins to form the transcription factor complex activator protein-1 (AP-1) [9]. With differential combinations of the FOS/JUN members, AP-1 binds to different promoters and enhancers to orchestrate multiple cellular and physiological processes in normal tissues. In various types of tumors, AP-1 is shown to promote tumorigenesis, tumor cell proliferation and motility [10–12]. Immunohistochemical (IHC) staining of clinical samples indicated high expression of FOSL1 in different solid tumors including bladder cancer [13], oesophageal cancer [11], and breast cancer [14]. Functionally, FOSL1 has been reported to play an important role in the tumorigenesis and progression of lung, prostate, colon, head and neck squamous cell carcinoma, and glioma [15, 16]. In breast cancer, higher levels of FOSL1 are often detected in the more aggressive and highly malignant subtypes, such as TNBC [17–19] and HER2-overexpressed subtype [20]. In addition, higher expression of FOSL1 was observed in the lymph nodes of metastatic breast cancer lesion as compared to non-metastatic tumors [21]. Overexpression of FOSL1 was shown to promote malignant phenotypes of TNBC in in vitro and in vivo studies [12]. High expression of FOSL1 predicts poor survival of patients with basal-like breast cancer, mutant KRAS lung cancer as well as pancreatic cancer [22, 23]. Mechanistically, it has been reported that FOSL1 acts as a direct transcriptional activator or repressor depending on the gene, by binding to distally located enhancers in TNBC cells [10]. However, TNBC-specific SE targeted by FOSL1 remains to be identified.

In our previous study, we have performed bioinformatics analysis to predict potential TFs which could bind to SE of TCOF1 gene. Here, by performing DNA pull down and mass spectrometry studies, coupled with our previous bioinformatics data, we identified candidate TFs which bind to TNBC-specific SE of TCOF1 gene. Among the TF candidates, FOSL1 was chosen for further validation, given its overexpression in most TNBC cases as well as its known function in determining TNBC aggressiveness [12, 21]. Using FOSL1 shRNAs, we provide evidence that FOSL1 drives SE-mediated TCOF1 expression and TNBC growth and stemness. We further demonstrated that the TCOF1 SE is activated by FOSL1. This work identifies TCOF1 as a direct transcriptional target of FOSL1, and highlights the potential of targeting FOSL1-SE-TCOF1 transcriptional program for therapeutic treatment of TNBC.

Results

Identification of transcription factors associated with TCOF1 super-enhancer

In our previous studies, we uncovered a TNBC-specific SE (SE324) that drives TCOF1 expression, and found enrichment of acetylation of histone H3 at lysine 27 (H3K27ac) signals in the constituent enhancer E1 region of SE324 in TNBC cell lines compared to non-TNBC cell lines [7, 8]. Furthermore, using FIMO to detect nucleosome-free regions and position frequency matrices from JASPAR database (http://jaspar.genereg.net/), we pred icted 127 TFs that potentially bind to SE324 [8]. In this study, we aimed to identify TFs that bind to the E1 region of TCOF1 SE and drive its expression. We first performed a DNA pull-down assay with a biotinylated TCOF1-E1 SE sequence followed by mass spectrometry analysis. 188 proteins were demonstrated to bind to the TCOF1-E1 region, of which 98 are DNA-binding proteins (Fig. 1A). We next combined the mass spectrometry data with our previous bioinformatics analysis of the 127 predicted TFs (Fig. 1B) [8]. By overlapping the TCOF1-E1-binding proteins with the predicted TFs, we identified 12 TFs, including FOSL1, FOSL2, JUNB, JUND, TP73, FOXK2, NR2F2, NF1A, RUNX1, TFAP2B, NR3C1 and HSF1 (Fig. 1C), many of which are implicated in tumorigenesis and cancer progression. To prioritize TFs for further examination of their function in driving TCOF1 expression via SE, the scores of motif occurrence were determined using the JASPAR database. FOSL2 and FOSL1 were shown to be the top two enriched motifs in TCOF1-E1 (Fig. 1D).

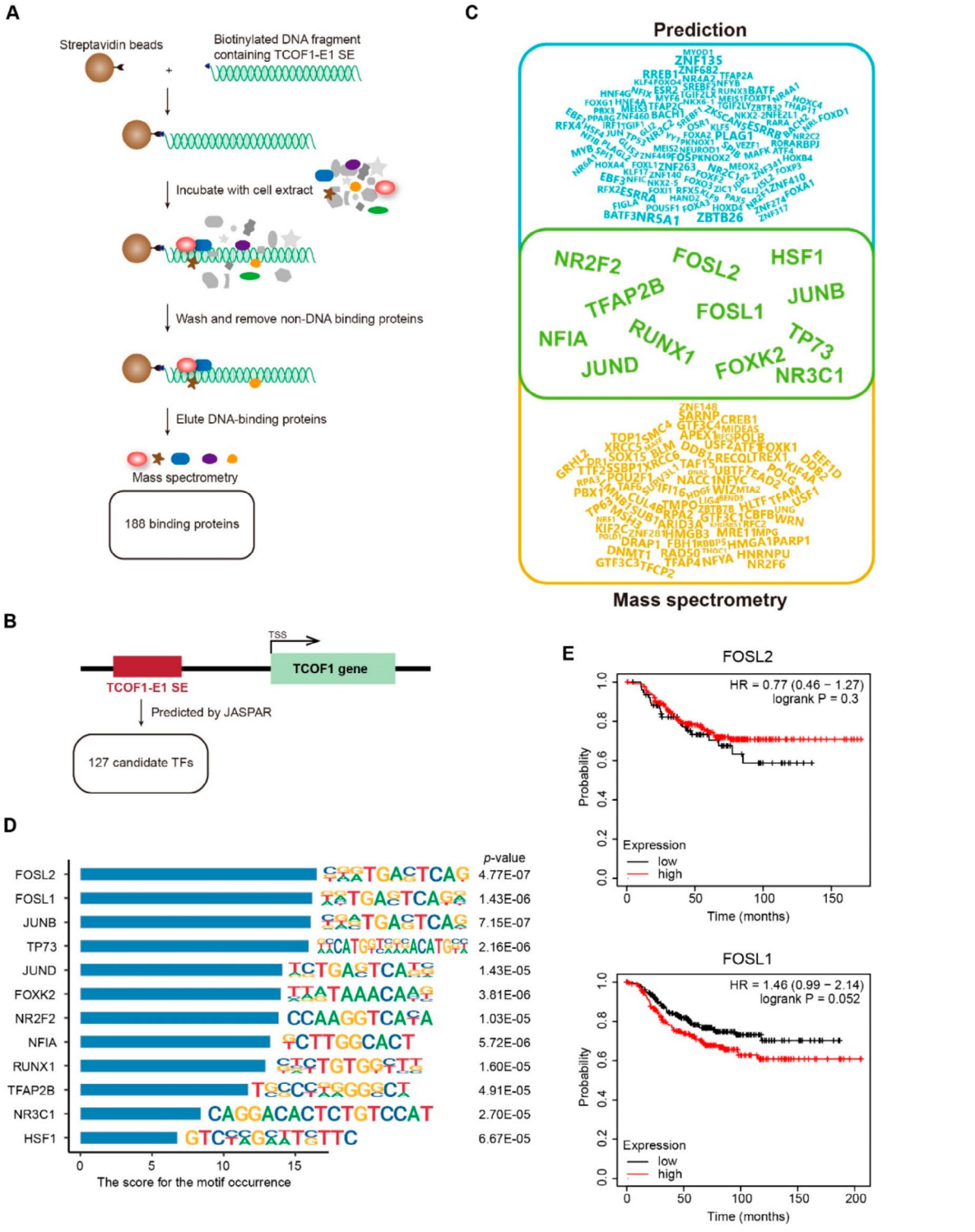

Fig. 1 Identification of TFs associated with TCOF1 SE. (**A**) Schematic diagram showing the workflow for DNA pull-down assay. (**B**) Diagram depicting the bioinformatics prediction of associated TFs. (**C**) Venn diagram shows TFs potentially binding to the TCOF1-E1 SE identified by bioinformatics analysis and mass spectrometry. The size of TFs uniquely found by bioinformatics prediction was proportionate to -log10 transformed *p*-value, and the size of TFs found by mass spectrometry only was in proportion to -log10 transformed BH-adjusted *p*-value. The box in blue represents the factors that were only predicted by bioinformatics. The box in yellow represents the factors that were only identified by mass spectrometry. The box in green represents the factors that were identified by both bioinformatics and mass spectrometry. (**D**) TF DNA motif analysis at TCOF1-E1 SE. The bar chart shows the score of enriched motif occurrence identified at TCOF1-E1 SE. (**E**) The overall survival curves of FOSL2 and FOSL1 in TNBC patients

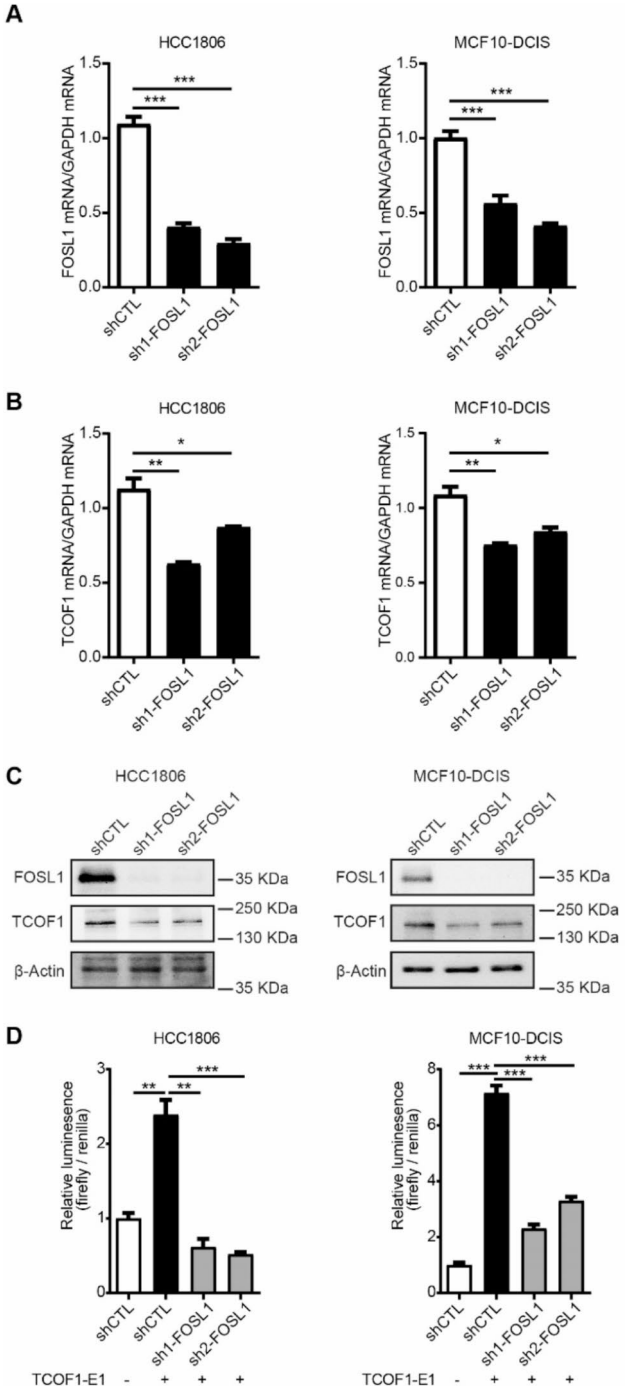

Fig. 2 FOSL1 knockdown reduces TCOF1 level and TCOF1 SE activity. (**A**) RT-qPCR verified the knockdown of FOSL1 mRNA in HCC1806 cells and MCF10-DCIS cells. Data, mean ± SEM: ***, $p < 0.001$ ($n = 3$). (**B**) RT-qPCR verified the downregulation of TCOF1 mRNA in HCC1806 cells and MCF10-DCIS cells knocked down FOSL1. Data, mean ± SEM: *, $p < 0.05$; **, $p < 0.01$ ($n = 3$). (**C**) Western blot of FOSL1 and TCOF1 in FOSL1-depleted HCC1806 cells and MCF10-DCIS cells. (**D**) SE activity of TCOF1-E1 in HCC1806 and MCF10-DCIS expressing FOSL1 or Control shRNAs was measured by dual-luciferase reporter assay. Data, mean ± SEM: **, $p < 0.01$; ***, $p < 0.001$ ($n = 3$)

Interestingly, FOSL1, but not FOSL2, is often detected in more aggressive and highly malignant subtypes, such as TNBC [10]. We also analyzed the overall survival of TNBC patients using the Kaplan–Meier plotter database. Although the results did not reach statistical significance, high expression of FOSL1 showed a trend towards poor prognosis in patients ($p = 0.052$) (Fig. 1E). Consistent with these findings, the expression of FOSL1 is positively correlated with TCOF1 expression in a gene expression dataset of breast cancer patients (Figure S1, TCGA-BRCA, $n = 1{,}100$). We, therefore, focused on FOSL1 for further investigation in the present study.

FOSL1 binds to TCOF1 super-enhancer region and upregulates TCOF1 expression level

To determine the functional role of FOSL1 in TCOF1 expression, we knocked down FOSL1 using a lentiviral-based shRNA system in two TNBC cell lines, HCC1806 and MCF10-DCIS. Data from RT-qPCR and Western blotting validated the efficient depletion of FOSL1 by two independent shRNAs [24, 25] (Fig. 2A and C). Upon FOSL1 knockdown, TCOF1 mRNA and protein expression levels were reduced significantly compared with the shCTL group (Fig. 2B-C). We next examined the effect of FOSL1 on TCOF1 SE activity using a luciferase reporter system. TCOF1-E1 SE was cloned into the pGL3-Promoter vector to generate the luciferase reporter pGL3-Promoter-TCOF1-E1. Potent transcriptional activities were observed in HCC1806 and MCF10-DCIS cells transfected with TCOF1-E1 compared to control pGL3-Promoter plasmids (Fig. 2D). In contrast, the depletion of FOSL1 abolished the luciferase reporter activity. These data suggested that FOSL1 acts as a TF of TCOF1 SE in TNBC cells.

To examine the binding of FOSL1 to TCOF1-E1 SE, we performed Chromatin Immunoprecipitation (ChIP)-qPCR using anti-FOSL1 antibody. Upon FOSL1 depletion by shRNA, FOSL1 enrichment levels on TCOF1 SE in HCC1806 and MCF10-DCIS cells were significantly reduced (Fig. 3A). In contrast, the binding of FOSL1 to the DNA region between TCOF1 SE and the transcription start site (TSS) of *TCOF1* gene (TCOF1-NEG) was much lower, and the binding was not reduced in FOSL1-depleted cells (Figure S2A). JQ1 is a Bromo- and Extra-Terminal domain (BET) inhibitor that shows promising anti-tumor potency in various cancers, including TNBC [26]. Our previous study has shown that JQ1 treatment resulted in decreased binding of BRD4 to TCOF1 SE as well as TCOF1 expression [8]. To examine if JQ1 modulates the binding of FOSL1 to TCOF1-E1 SE region, we performed ChIP-qPCR in JQ1- or vehicle-treated TNBC cells. JQ1 treatment significantly inhibited the binding of FOSL1 to SE of TCOF1 (Fig. 3B, Figure S2B), and reduced the expression of TCOF1 as well as FOSL1 (Fig. 3C).

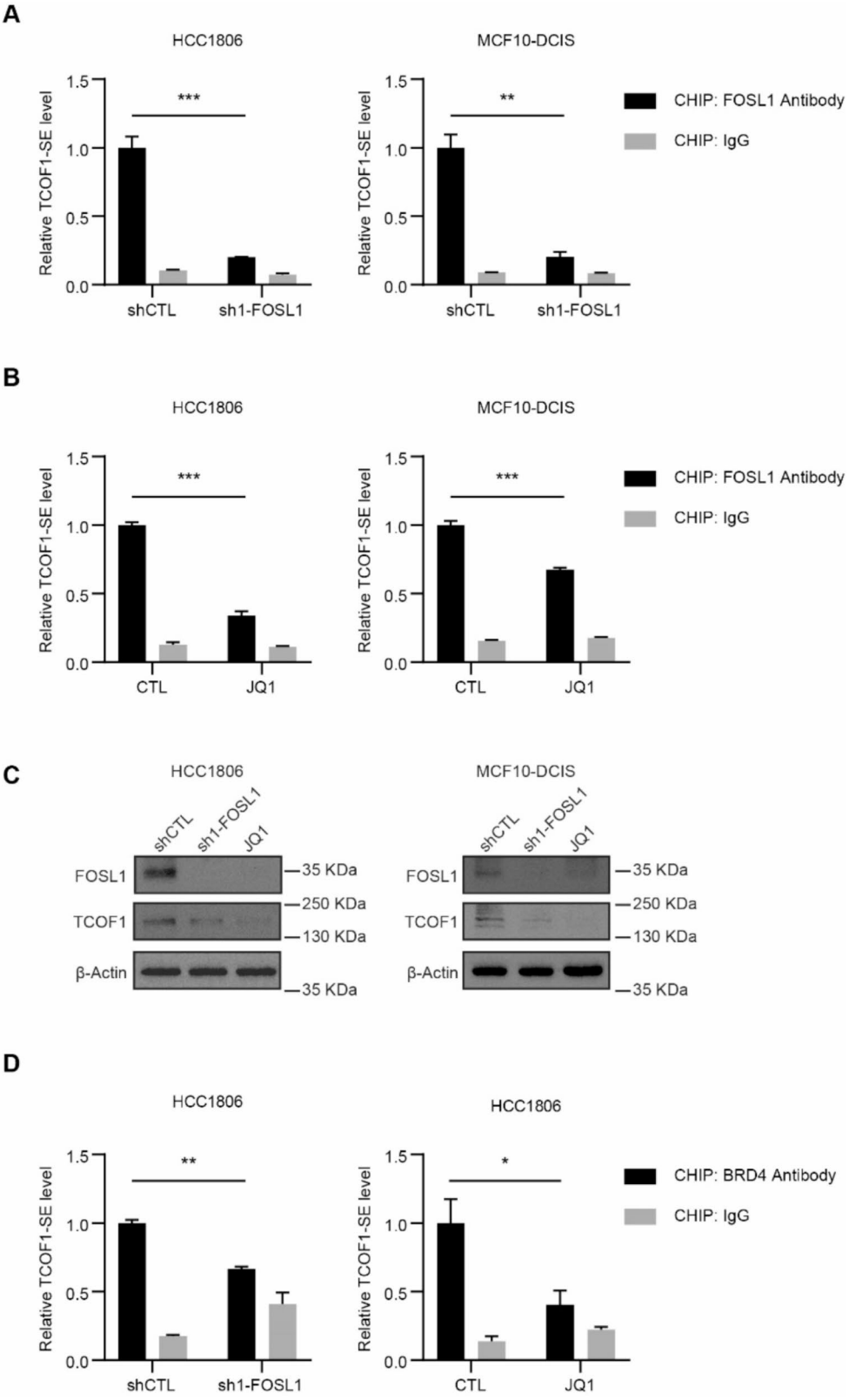

Fig. 3 FOSL1 binds to TCOF1-E1 SE and upregulates TCOF1 expression level. (**A**) FOSL1 and isotype IgG ChIP-qPCR in FOSL1-depleted HCC1806 and MCF10-DCIS cells using primers amplifying TCOF1-E1 SE. Data, mean ± SEM: **, $p < 0.01$; ***, $p < 0.001$ ($n = 3$). (**B**) FOSL1 and isotype IgG ChIP-qPCR in HCC1806 and MCF10-DCIS cells with or without JQ1 treatment (1 μM). Data, mean ± SEM: ***, $p < 0.001$ ($n = 3$). (**C**) Western blot of FOSL1 and TCOF1 in FOSL1-depleted cells or JQ1-treated cells. (**D**) BRD4 and isotype IgG ChIP-qPCR in FOSL1-depleted HCC1806 cells and JQ1-treated HCC1806 cells. Data, mean ± SEM: *, $p < 0.05$; **, $p < 0.01$ ($n = 3$)

These data indicated that FOSL1 binds to TCOF1-E1 and mediates the overexpression of TCOF1 via SE. In addition, ChIP-qPCR using anti-BRD4 antibody showed that the BRD4 enrichment in TCOF1 SE was reduced by FOSL1 knockdown or JQ1 treatment (Fig. 3D), whereas the binding of BRD4 to TCOF1-NEG was not affected (Figure S2C). We next investigated if FOSL1 plays a role in activating TCOF1-E1 SE. Using ChIP assay for assessing H3K27ac signals of TCOF1-E1 SE in TNBC MDA-MB-231 cells, we showed that overexpression of FOSL1 resulted in a marked increase of H3K27ac levels in TCOF1-E1 (Fig. 4A), as well as TCOF1 expression (Fig. 4B and C). These results demonstrated that FOSL1 not only acts as a TF where it binds to the TCOF1-E1 SE region, but also contributes to the epigenetic activation of the SE, resulting in TCOF1 overexpression in TNBC cells.

FOSL1 silencing inhibits viability and stemness of TNBC cells

To investigate the functional significance of FOSL1 in TNBC cells, we examined the cell morphology and viability of FOSL1-depleted and control cells. In cells expressing FOSL1 shRNAs, cell swelling and cytoplasmic vacuoles, signs of cell apoptosis [27], were prominent compared with control cells (Fig. 5A). We then tested the effects of FOSL1 on cell viability using CellTiter-Glo® 2D assay. Depletion of FOSL1 significantly inhibited the cell viability of HCC1806 and MCF10-DCIS cells (Fig. 5B). In contrast, FOSL1 depletion only led to a mild reduction of non-TNBC T47D cell viability, which agrees with the fact that FOSL1 is minimally expressed in non-TNBC cells and that FOSL1 shRNAs had marginal effect on TCOF1 expression (Figure S3).

To more accurately assess the roles of FOSL1 in regulating phenotypes that govern tumor growth in vivo, we performed spheroid morphogenesis assay in 3D culture with TNBC line HCC1806. As shown in the representative images, FOSL1 silencing inhibited the growth of TNBC spheroids (Fig. 6A). We also quantified the viability of cells in 3D spheroids using CellTiter-Glo® 3D assays, and showed that knockdown of FOSL1 by shRNA1 and shRNA2 resulted in 95% and 80% reduction of cell viability, respectively (Fig. 6A). Given the high degree of heterogeneity of TNBC cells and the enrichment of cancer stem cells that contribute to high malignancy, recurrence and drug resistance, we further examined the consequence of FOSL1 depletion on the stemness of TNBC cells. In mammosphere formation assays, we showed that the mammosphere number was reduced significantly upon FOSL1 knockdown (Fig. 6B). Next, we tested the effect of FOSL1 on aldehyde dehydrogenase (ALDH) expression and activity, a marker of breast cancer stem cells (CSCs). Knockdown of FOSL1 markedly decreased the percentage of ALDH ^{high} population in HCC1806 cells (Fig. 6C). The expression levels of ALDH1A1 were reduced by 50% upon FOSL1 silencing (Fig. 6D). In addition, the percentage of CD44^{high}/CD24$^{-/low}$ cells, a population of CSCs in TNBC lines and breast tumors, was decreased in FOSL1-depleted HCC1806 cells (Figure S4). Importantly, over-expression of TCOF1 restored mammosphere formation of FOSL1-depleted cells (Fig. 6E). Recently, microfluidics with cell-laden microgel approach has emerged as a powerful tool

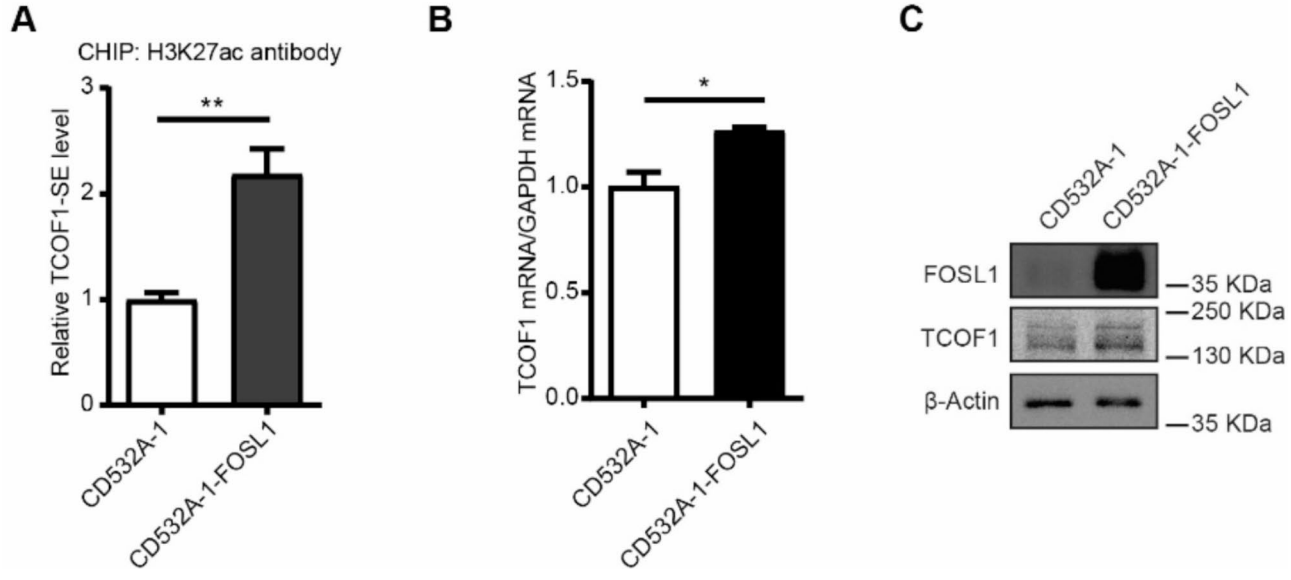

Fig. 4 Overexpression of FOSL1 promotes TCOF1 expression. (**A**) H3K27ac ChIP-qPCR in MDA-MB-231 cells overexpressing FOSL1 using primers amplifying TCOF1-E1 SE. Data, mean ± SEM: **, $p < 0.01$ ($n = 3$). (**B**) RT-qPCR for assessing TCOF1 mRNA levels in MDA-MB-231 cells overexpressing FOSL1. Data, mean ± SEM: *, $p < 0.05$ ($n = 3$). (**C**) Western blot of FOSL1 and TCOF1 in MDA-MB-231 cells overexpressing FOSL1

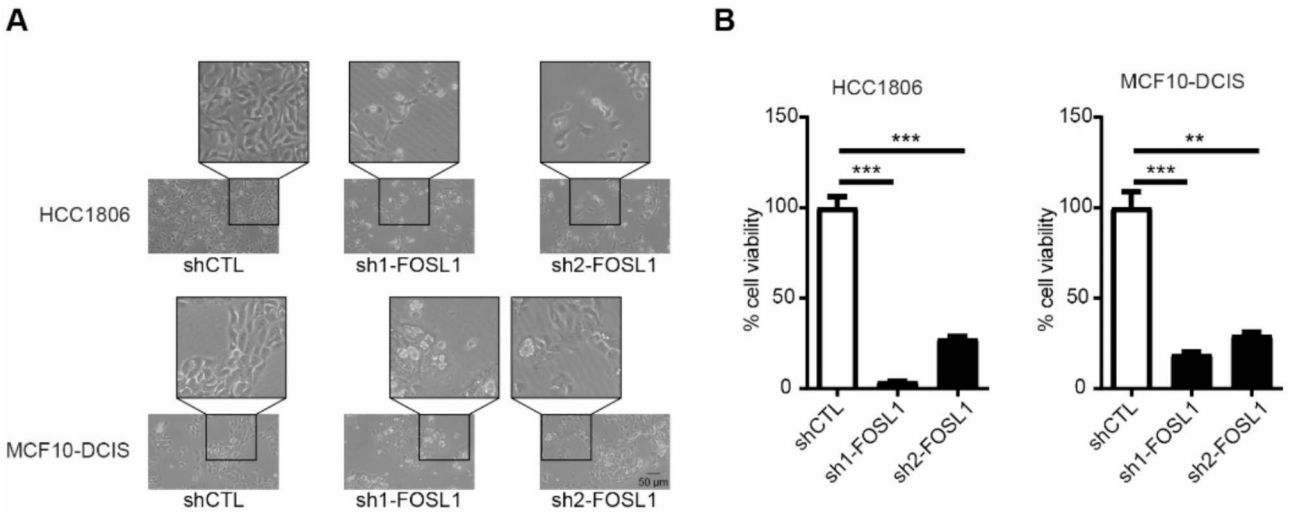

Fig. 5 FOSL1 silencing inhibits TNBC cell viability. (**A**) HCC1806 and MCF10-DCIS cell morphology after FOSL1 silencing. (**B**) HCC1806 and MCF10-DCIS cells expressing FOSL1 or control shRNAs were cultured in 2D for 3 days, followed by CellTiter-Glo® two-dimensional (2D) cell viability assay. Data, mean ± SEM: **, $p < 0.01$; ***, $p < 0.001$ ($n = 3$)

to study various mechanisms of tumorigenesis including cancer stemness, invasion and intercellular signaling. By precise fabrication and tailored microenvironments, it allows modeling of cancer initiation and progression processes [28]. Here, we used a droplet-based microfluidic device to fabricate the single-cell-laden microcapsules, in which only single cancer stem cells survive and grow into mammospheres (Fig. 7A). We showed that single cells were successfully encapsulated in the microgel, where at least 95% of the encapsulated cells are single in the microgel (Fig. 7A). Compared to the classical mammosphere assay, this cell-laden microgel approach provides the advantage of preventing cancer stem cells or mammospheres from clumping and merging with each other. HCC1806 cells expressing control or FOSL1 shRNAs were loaded into the single-cell-laden microcapsules and individual cancer stem cells were allowed to grow into mammospheres. Viability of cells were assessed by live/dead co-staining with Calcein-AM and PI at the indicated time points (Fig. 7B). Living cells exhibited green fluorescence with Calcein-AM staining and dead cells showed red fluorescence with PI staining. As shown in Calcein-AM staining of the representative images, controlled mammospheres are increased in size over the period of 10 days (Fig. 7B). In contrast, mammospheres with FOSL1 shRNAs remained small. Majority of cells in the controlled mammospheres exhibited green fluorescence, whereas most of the cells with FOSL1 depletion exhibited red fluorescence (Fig. 7B). Data from the bar graphs demonstrate that depletion of FOSL1 significantly inhibited single-cell-derived mammosphere formation and growth in microcapsules (Fig. 7C). These data suggest that FOSL1 promotes growth of TNBC spheroids and stemness properties of TNBC cells.

Discussion

Aberrant activation of SE has been observed in different types of cancers, but the underlying regulators and mediators, especially TFs which preferentially bind to the SE region, remain largely elusive [29]. With combinatorial epigenetic and transcriptomic analyses, we recently uncovered the pivotal role of SEs in characterizing breast cancer subtypes. In addition, multiple oncogenes, including MET, FOXC1, ANLN, and TCOF1, were demonstrated to be driven by TNBC-specific SEs. We further identified their functional roles and clinical significance in TNBC [8, 30]. In the present study, we showed that the activation of a TNBC-specific SE and the overexpression of its associated oncogene, TCOF1, is mediated by TF FOSL1.

TCOF1 has emerged as a critical modulator for multiple biological processes, including ribosome biogenesis [31], protein translation [32], DNA damage response [33], as well as determining oncogenic properties [8]. The molecular mechanism that regulates TCOF1 expression, however, remains to be elucidated. Here, we explored the upstream regulatory mechanism underlying transcriptional upregulation of TCOF1 in TNBC. We combined DNA pull-down assay and bioinformatics analysis to identify 12 potential TFs binding to the TNBC-specific SE associated with TCOF1 gene. Interestingly, 4 out of these 12 TFs, including FOS (FOSL1 and FOSL2) and JUN (JUNB and JUND), belong to AP-1 family members. To regulate transcriptional activity, AP1 proteins form dimeric complexes which are composed of FOS, JUN, ATF, and MAF family proteins [34]. Given the elevated expression of FOSL1 is often observed in human cancers and is correlated with tumor aggressiveness, we focused on validating the functional role of FOSL1 in driving

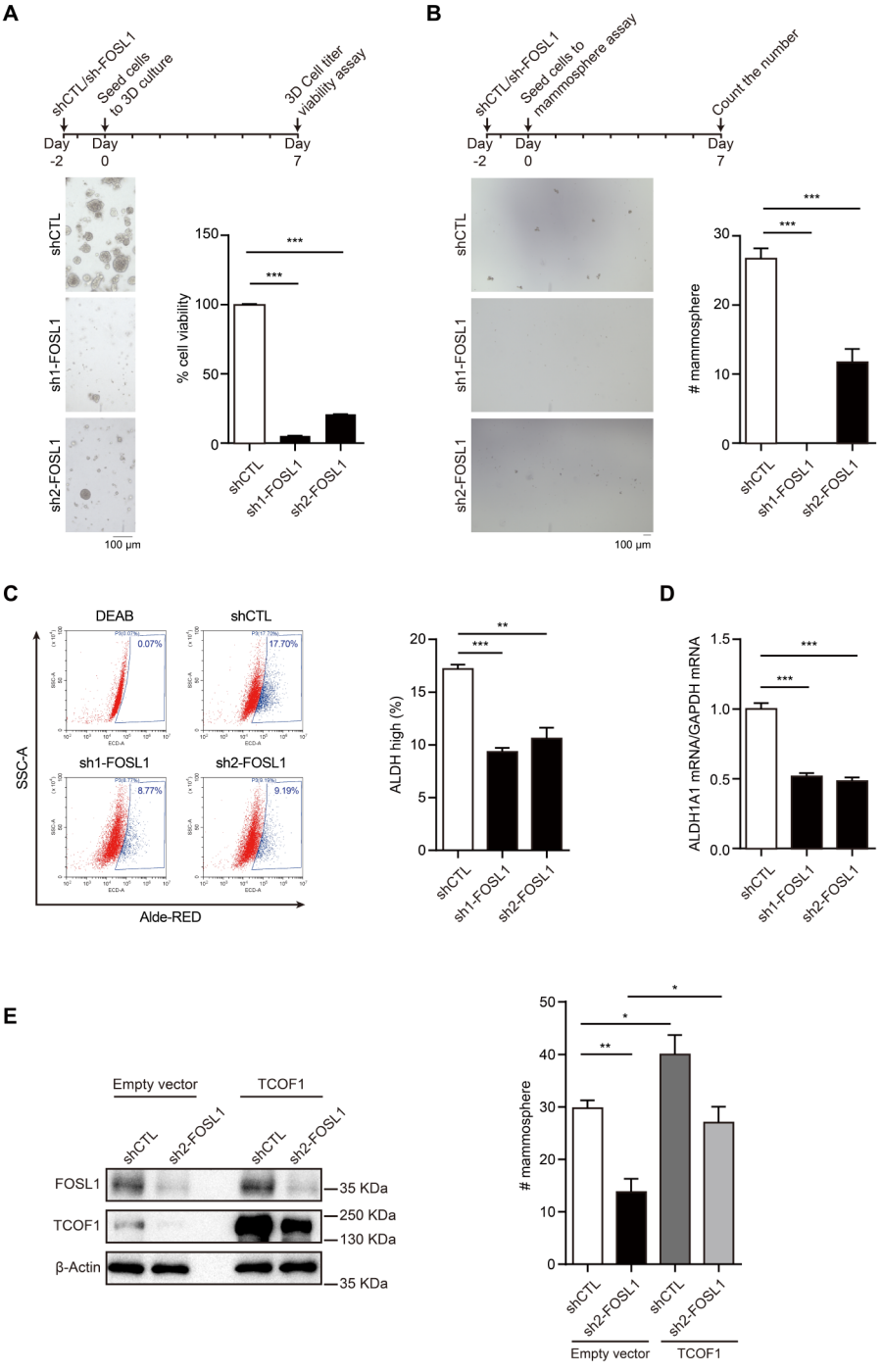

Fig. 6 Knockdown of FOSL1 inhibits spheroid growth and stemness of TNBC. (**A**) Schematics of FOSL1 knockdown by lentiviral infection and 3D culture. HCC1806 cells expressing FOSL1 or control shRNAs were cultured in 3D for 7 days and images were captured. Bar graphs depict the growth of 3D spheroids. Data, mean ± SEM: ***, $p < 0.001$ ($n = 3$). (**B**) Schematics of FOSL1 knockdown by lentiviral infection and mammosphere formation assay. HCC1806 cells expressing FOSL1 or control shRNAs were seeded for mammosphere formation assay. Representative images of mammosphere are shown and the bar graph depicts the numbers of mammosphere. Data, mean ± SEM: ***, $p < 0.001$ ($n = 3$). (**C**) ALDH activity of cells derived from HCC1806 with or without FOSL1 knockdown, measured by AldeRed ALDH Detection assay. Cell populations with high ALDH activity were quantified and depicted in bar graphs. Data, mean ± SEM: **, $p < 0.01$; ***, $p < 0.001$ ($n = 3$). (**D**) RT-qPCR showed the mRNA level of ALDH1A1 in control or FOSL1-depleted HCC1806 cells. Data, mean ± SEM: ***, $p < 0.001$ ($n = 3$). (**E**) HCC1806 cells expressing TCOF1 or empty vector were infected with control or FOSL1 shRNAs. Cells were continued to culture for 2 days, and then subjected to Western blot analysis for FOSL1 and TCOF1 or mammosphere formation assay. Data, mean ± SEM: *, $p < 0.05$ ($n = 3$)

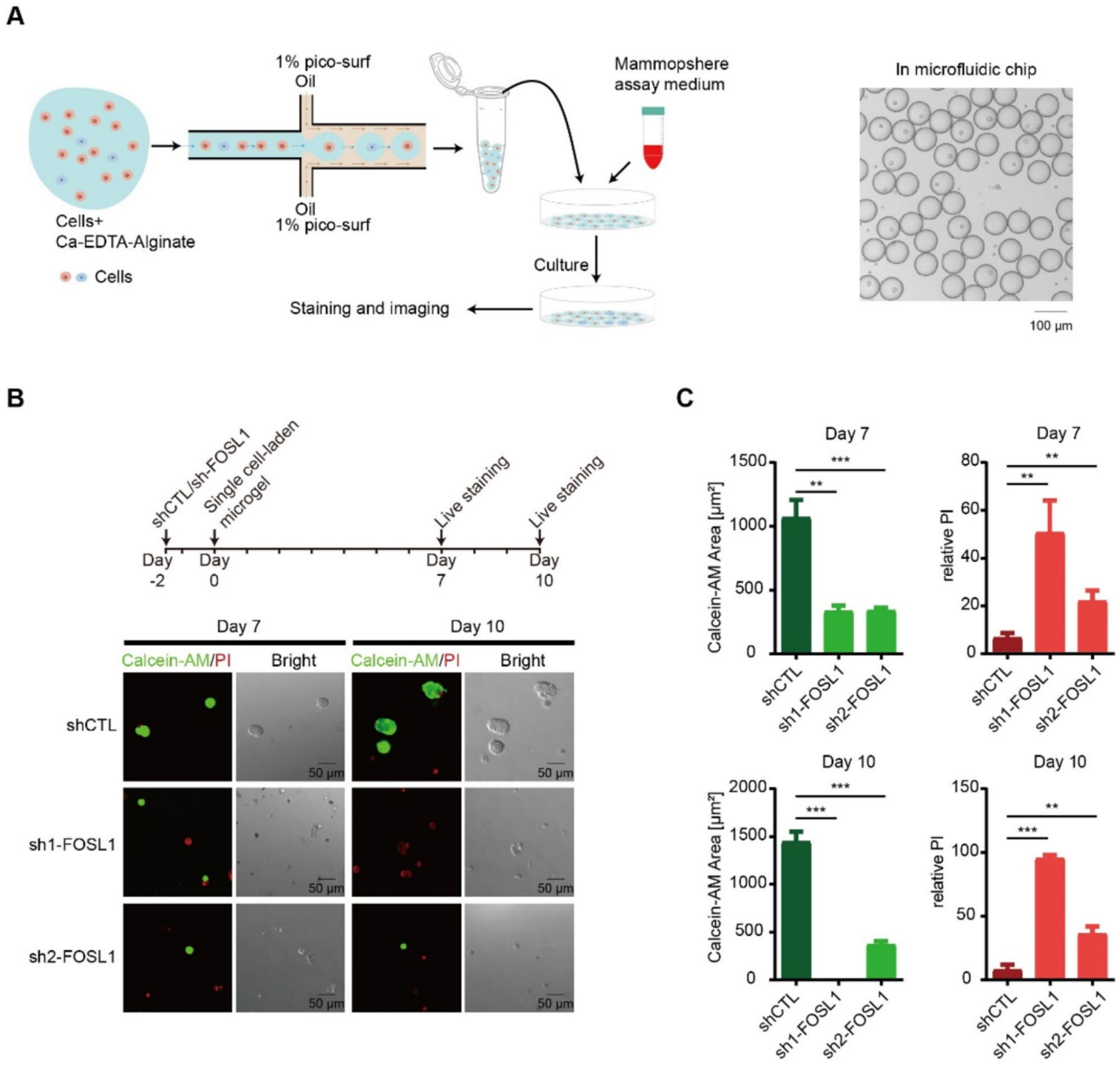

Fig. 7 Knockdown of FOSL1 inhibits stemness of TNBC in single-cell-laden microcapsules. (**A**) Schematic diagram (left) showing the workflow for forming single-cell-laden microcapsules. Representative image (right) showing that single cells were encapsulated in microgels. (**B**) Schematics of knocking down FOSL1 for live staining in single-cell-laden microcapsules. HCC1806 cells expressing FOSL1 or control shRNAs were encapsulated in microgel droplets and cultured in mammosphere medium for the indicated time. Live staining was performed and images were captured. (**C**) Bar graphs show the size of live mammospheres (left panel) and dying mammosphere percentage (right panel). Data, mean ± SEM: **, $p < 0.01$; ***, $p < 0.001$ ($n = 3$)

TCOF1 expression in TNBC via SE. Previous studies have demonstrated that FOSL1 binds to promoters and distant enhancers of multiple genes to promote their expression [35, 36]. For example, RNAi-mediated down-regulation of FOSL1 inhibits the expression of a panel of genes involved in migration, invasion and proliferation in TNBC cell lines, including MDA-MB-231 and BT549 cells [10, 12]. Our data exemplify the regulatory role of FOSL1 and showed that FOSL1 mediates the overexpression of TCOF1 by binding to SE. RNAi-mediated silencing of FOSL1 led to reduced TCOF1 transcription and translation, and ChIP-qPCR data confirmed the association of FOSL1 with the E1 region of TCOF1 SE. Another important finding of our study is that FOSL1 not merely acts as a mediator for bridging the SE to promoter for gene expression, it plays an important role in activating the SE, providing a mechanism for the enhanced SEs in TNBC. Interestingly, in MCF10-DCIS cells, FOSL1 knockdown has a more potent effect on TCOF1 protein levels compared to its mRNA levels. It has been shown

that FOSL1 promotes transcription of oncomiRs such as miR-221/222 [37], and miR-221/222 can bind to KIT mRNA, blocking its translation [38]. It will be interesting to test in the future if FOSL1 modulates oncomiRs to affect TCOF1 translation. In ovarian cancer, FOSL1, a well-recognized ERK downstream target [39], was shown to promote ERK/JNK signaling to form a positive feedback loop [40]. We will test if TCOF1 can be targeted by MEK/ERK-associated kinases, potentially stabilizing the protein, in future studies.

BET family proteins, particularly BRD4, serve as epigenetic readers that recognize and interact with acetyllysine residues on histone, and recruit the Mediator complex, RNA polymerase II, and transcription elongation factor to initiate RNA transcription and elongation [41]. JQ1, a selective inhibitor of BET proteins, competes with acetyl-binding pockets of BRD4 and modulates RNA transcription. As demonstrated in recent studies, JQ1 inhibits SEs and thereby the transcription of oncogenes in various cancers [42, 43]. In this study, ChIP-qPCR data showed that JQ1 treatment inhibited the binding of FOSL1 to the E1 region of TCOF1 SE, supporting the direct effect of JQ1 on the TCOF1 SE. In future studies, the specific binding location can be identified by mutating the FOSL1 binding motif in the TCOF1-E1. It is worthwhile to note that, in addition to TCOF1, JQ1 treatment led to a reduction of FOSL1 protein levels. Others have shown that JQ1 treatment suppresses FOSL1 expression by displacing BRD4 from the FOSL1 promoter and enhancer regions [44]. This is likely that our observed results of JQ1 in modulating TCOF1 expression are contributed by its effects on both the FOSL1 and TCOF1 gene locus. It is also known that JQ1 can inhibit MYC transcription. Given MYC can bind to the FOSL1 enhancer region thereby promoting its transcriptional activation [45], JQ1's effect on FOSL1 expression could also be mediated through MYC. Nevertheless, our biochemical studies provided strong evidence that FOSL1 binds to TCOF1 SE to enhance the transcription of TCOF1. This study focused on determining the role of FOSL1 as a TF to regulate TCOF1 gene expression. It would be interesting to examine the functional role of other AP1 candidate TFs in dimerizing with FOSL1 to modulate TCOF1 in future studies.

The role of FOSL1 in tumorigenesis of various tumors has been widely studied. In squamous cell carcinoma, FOSL1 regulates cancer stem cell self-renewal and promotes metastasis [46]. In ameloblastoma, FOSL1 enhances tumor growth and invasiveness by modulating kinetochore metaphase signaling and epithelial-to-mesenchymal transition (EMT) [47]. FOSL1 has also been reported to modulate the malignant aggressiveness of colorectal carcinoma [48]. In TNBC, FOSL1 plays important roles in regulating tumor cell proliferation, EMT, stemness, invasion, metastatic potential, and drug resistance [22, 49, 50]. A FOSL1-dependent gene expression signature was characterized in mesenchymal breast cancer cells. This FOSL1 classifier was shown to accurately predict recurrence of breast cancer [51]. Interestingly, TCOF1 was not included among the FOSL1 top-regulated genes. A possible reason is that basal-like TNBC cells were examined in our study, whereas the published FOSL1 classifier was conducted in mesenchymal TNBC cells. Mechanistically, FOSL1 has been shown to induce EMT of mammary epithelial cells by modulating TGFβ signaling and Zeb1/2 expression [52]. These studies support the tumor-promoting function of FOSL1 that we observed in our study. We showed that FOSL1 promotes TNBC spheroid growth and stemness properties. In 2D and 3D cell viability assays, FOSL1 depletion significantly inhibited cell proliferation and viability with a dramatic change in cell morphology. Using mammosphere formation assays, CSC markers, as well as single-cell-laden microcapsules, we also demonstrated the role of FOSL1 in modulating the stemness of TNBC cells. In summary, this study elucidates a FOSL1-mediated SE mechanism for the upregulation of oncogene TCOF1 in TNBC (Fig. 8). The FOSL1-TCOF1 axis may be exploited as prognostic biomarkers and therapeutic targets for TNBC treatment.

Experimental procedures

Cell culture

HCC1806, MDA-MB-231, T47D and HEK293T cells were obtained from ATCC. MCF10-DCIS cells were provided by Kornelia Polyak (Harvard Medical School, USA). HCC1806 cells were maintained in RPMI 1640 medium (Gibco) containing 10% fetal bovine serum

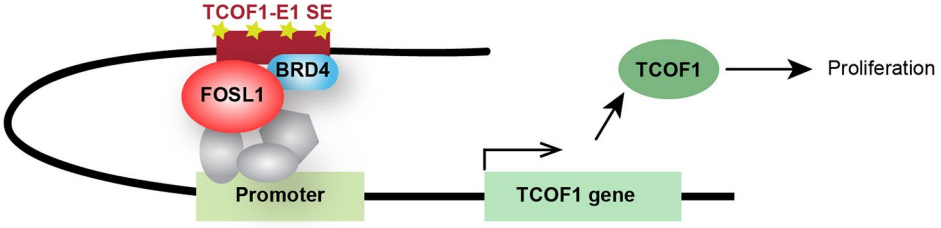

Fig. 8 Proposed model of the role and mechanism of FOSL1 in activating TCOF1 SE and mediating overexpression of TCOF1 via SE

(FBS; Clontech). MDA-MB-231, T47D and HEK293T cells were cultured in Dulbecco's Modified Eagle medium (DMEM; Gibco) containing 10% FBS. MCF10-DCIS was maintained in DMEM/F-12 (Gibco) supplemented with 5% horse serum, 20 ng/ml epidermal growth factor (EGF), 10 μg/ml insulin, 100 ng/ml final cholera toxin and 500 ng/ml hydrocortisone. All cell lines are regularly tested for mycoplasma contamination. They have been tested for authentication using short tandem repeat profiling and passaged for <6 months.

Lentiviral vector infection

The shRNAs (sequences are listed in Supplementary Table 1) specific targeting FOSL1 mRNA were ligated to the lentiviral vector pLKO.1 digested by AgeI (NEB, R3552S) and EcoRI (NEB, R3101s) restriction enzyme to generate plasmids (pLKO.1-sh1/2-FOSL1). For overexpression of exogenous FOSL1 and TCOF1, CDS of FOSL1 and TCOF1 was synthesized and cloned into vector CD532A-1 by GENEWIZ. To prepare lentiviral supernatants, 10 μg lentiviral vectors (pLKO.1-shRNA CTL, pLKO.1-sh1-FOSL1, pLKO.1-sh2-FOSL1, CD532A-1, CD532A-1-FOSL1, CD532A-1-HA-TCOF1) were co-transfected with 7 μg psPAX2 and 2.4 μg VSV-G vectors to HEK293T cells in a 10-cm plate, using polyethylenimine as transfection reagent. Sixty hours post transfection, the supernatants containing lentiviruses were collected and filtered by 0.45 μm syringe filters (Thermo fisher, 7232545). For infection of lentivirus to TNBC cells, 0.15–0.2 ml lentivirus with 5 μg/ml polybrene was added to cells for 12–24 h in a well of 6-well plate. After around 48–60 h of infection with lentivirus, cells were used for protein and RNA extraction or next CellTiter-Glo® 3D and 2D Cell Viability Assay.

Overall survival analysis

The Kaplan-Meier plotter database (https://kmplot.com/analysis/) was used to analyze the prognosis of FOSL1 and FOSL2. The patients were split by auto-selected best cutoff with a follow-up time included. The TNBC (basal) subtype was chosen in the StGallen. All datasets were included for the analysis. The Kaplan-Meier survival plots, the hazard ratio, 95% confidence interval, and log rank *P*-value were displayed.

Quantitative reverse transcription-PCR (RT-qPCR)

Total RNA from HCC1806 and MCF10-DCIS cells in 6-well plates was extracted using the RNeasy Plus Mini Kit (Qiagen, #74134) according to the manual. Reverse transcription (RT) was performed using TaqMan Reverse Transcription Reagents (Applied Biosystems, N8080234). Quantitative RT-PCR was performed using a QuantStudio 12 K Flex Real-Time PCR System (Applied Biosystems). Relative expression levels of target genes were normalized to GAPDH. All primers used in the RT-qPCR are listed in Supplementary Table 1.

Chromatin immunoprecipitation (ChIP)-qPCR

ChIP-qPCR was performed following the previously described methods [8]. Briefly, HCC1806, MCF10-DCIS or MDA-MB-231 cells were cross-linked with 1% PFA at room temperature for 5 min, followed by washing twice with PBS. Cells were scraped into 1 ml ChIP lysis buffer (1% Triton, 0.1% Na-deoxycholate, 50 mM HEPES, pH 7.5, 140 mM NaCl, 1 mM EDTA, 1× proteinase inhibitor cocktail) and incubated on ice for 15 min. The lysate of cells was sheared using Bioruptor Plus (Diagenode, UCD-300 TM) for 30 cycles (30 s ON and 30 s OFF at high power) to shear the chromatin, followed by two sequential centrifugations (10,000 × g for 5 and 15 min at 4 °C) to collect the soluble chromatin. The lysate was then incubated with the FOSL1 antibody, BRD4 antibody, H3K27ac antibody or isotype IgG at 4 °C overnight, followed by incubating with Protein G Sepharose (GE Healthcare, 17061802) pre-washed with ChIP lysis buffer for 1 h at 4 °C. After washing, samples were treated with 10% chelex (Bio-Rad, 142–1253) and then with 20 mg/ml Proteinase K (NEB, P8107S), followed by centrifugation. The precipitated DNA samples were measured by qPCR using Applied Biosystems QuantStudio 3 Real-Time PCR System. Primers for ChIP-qPCR are listed in Supplementary Table 1.

DNA pull-down assay

The TCOF1-E1 SE was amplified by PCR using 5′-biotinylated forward primer. PCR Primers of biotinylated-DNA of TCOF1-E1 SE are listed in Supplementary Table 1. PCR product was purified by QIAquick Gel extraction kit (Qiagen #28706) and immobilized on Streptavidin-Agarose beads (Thermo Scientific) in binding buffer (20 mM HEPES (pH 7.5), 2.5 mM KCl, 20% glycerol, 1 mM DTT, 0.02% NP40) for 30 min at room temperature, followed by wash once. Cells lysate in TNTE buffer (50 mM Tris/HCl (pH 7.6), 150 mM NaCl, 1 mM EDTA, 0.5% Triton X-100, protease and phosphatase inhibitors) was centrifuged at 13,000 g for 10 min at 4 °C. The lysate was incubated with the beads-biotinylated DNA complex, with or without 10 μg poly-dIdC (Sigma) used as a competitor for nonspecific DNA binding proteins, in a total volume of 1.4 ml, and incubated for 6 h at 4 °C. For samples subjected to sodium dodecyl sulfate-polyacrylamide gel electrophoresis (SDS-PAGE), complexes were washed 3 times with binding buffer. For samples used for mass spectrometry for protein identification, complexes were washed twice with binding buffer and three times with 50 mM ammonium bicarbonate.

CellTiter-Glo® three-dimensional (3D) and two-dimensional (2D) cell viability assays

3D and 2D cell viability were determined as previously described [8]. Briefly, for 3D cultures, growth factor-reduced Matrigel (Corning) was used to coat 96-well plates (Corning # 3610). Cells were seeded to the Matrigel-precoated 96-well plates in assay medium (relevant complete medium with 2% Matrigel supplement), with a density of 2000 cells per well, and allowed to grow in 5% CO2 humidified incubator at 37℃ for 7 days to form spheroids. To quantify spheroid viability, CellTiter-Glo® 3D Cell Viability Assay (Promega #G9682) was performed under the instruction of the Kit manual. For assessment of 2D cell viability, cells were directly seeded to 96-well plate, with a density of 4000 cells per well, and cultured for 3 days. CellTiter-Glo® Luminescent Cell Viability Assay (Promega #G7571) was used to quantify 2D cell viability according to the manufacturer's instructions. The bioluminescence signal was detected by a Synergy™ H1 Microplate Reader (BioTek).

Western blot

Total protein extracts were collected by lysing cells in EBN buffer (0.5% NP-40, 120 mM NaCl, 50 mM Tris-HCl (pH 7.4), proteinase inhibitor cocktail, 50 nM calyculin, 2 mM EDTA, 2 mM EGTA, 1 mM sodium pyrophosphate, 20 mM sodium fluoride) on ice for 30 min, followed by centrifugation at 13,000 × g at 4 °C for 10 min. Bio-Rad protein assay reagents (Bio-Rad, 5000114 and 5000113) were applied for the detection of protein concentration and the absorbance was read by a Synergy™ H1 Microplate Reader (BioTek). Then, 10 μg of protein was resolved by 10% SDS-PAGE followed by transfer to a nitrocellulose membrane. After blocking with 5% fat-free milk in TBST for 1 h, membranes were probed with indicated primary and secondary antibodies followed by enhanced chemiluminescence substrate (Pierce). The primary antibodies used were anti-FOSL1 (CST, # 5281T), anti-TCOF1 (sigma, # HPA038237), and anti-β-actin (CST, # 3700 S).

Dual-luciferase reporter assay

TCOF1-E1 was amplified from genomic DNA by PCR and cloned to firefly luciferase reporter pGL3-Promoter vector (Promega, #E1761). Plasmid pGL3-Promoter-TCOF1 E1 was co-transfected with pRL-TK vector (Promega, #E2241) into HCC1806 or MCF10-DCIS cells using FuGENE 6 transfection reagent (Promega, #2693). A pRL-TK vector plasmid expressing renilla luciferase was used as an internal transfection control. Two days after transfection, the Dual-Glo® Luciferase Assay System Kit (Promega, #E2920) was used to quantify luminescence signal. The firefly luciferase signal was first normalised to the renilla luciferase signal and then normalised to the empty pGL3-promoter plasmid signal.

Mammosphere formation assay

HCC1806 cells were seed to ultra-low attachment 6-well plate with cell density of 2000 cells per well and cultured in mammosphere assay medium (DMEM/F12 added with 2% B27 (Gibco, 12587010), 20 ng/mL FGF (PeproTech, 100-18B), and 20 ng/ml EGF (R&D, 236-EG)). Seven days after culturing, images of mammospheres were captured by Nikon Eclipse Tis2 microscope. Number of mammospheres with diameter ≥ 50 μm were counted using Nikon NIS-Elements D software.

AldeRed ALDH detection assay

The ALDH activity of cells was assessed using AldeRed ALDH Detection Assay kit (Merk, SCR150) following the manufacturer's instructions. Briefly, cells cultured in 2D were trysinized and collected. After washing, 2×10^5 cells were incubated with AldeRed reagent and verapamil for 35 min at 37℃ in the dark. Subsequently, the cells were centrifuged, and the pellets were resuspended in 500 μl ice-cold AldeRed buffer while kept on ice. The signal of AldeRed was then measured using Beckman Coulter CytoFLEX S Flow cytometer analyser with the ECM detector (610/20 BP). Diethylaminobenzaldehyde (DEAB), the ALDH inhibitor, was used as negative control testing to assess the background fluorescence.

CD44/CD24 Flow cytometry

One million cells in stain buffer (PBS with 2% serum, 0.2 mM EDTA, and 0.015% NaN_3) were incubated with CD44-PE (BD, 555479) and CD24-647 (BD, 561644) or isotype control IgG-PE (eBioscience, 12-4732-42) and IgG-647 (BD, 557715) at 4℃ for 30 min, protected from light. The cells were then washed and analyzed using a Beckman Coulter CytoFLEX S Flow cytometer. The threshold for positive signals is set according to the negative control of the isotype control IgG.

Fabrication of single-cell-laden microcapsules with droplet-based microfluidic device

A droplet-based microfluidic chip with a 50 μm thickness was fabricated by conventional photolithography for preparing single cell-laden microgels. After the fabrication of the device, a hydrophobic treatment was made on the surface of microchannel by 0.1% (v/v) of 1 H,1 H,2 H,2 H-perfluorododecyltrichloro (sigma) in Novec™ 7500 (3 M). To fabricate alginate microgels,1% (wt) alginate solution containing 50 mM Ca-EDTA was used as the internal phase, whereas the external phase was 1% (v/v) pico-surf in Novec™ 7500. Flow rates for internal and external phases were 0.15 and 0.45 ml per hour, respectively. After the formation of droplets

containing single cell in microfluidic channels, the emulsions were collected in Eppendorf tubes and crosslinked with 0.05% (v/v) acetic acid for 2 min before demulsification by 20% (v/v) of perfluorooctanol solution (Sigma). The crosslinked alginate microgels were collected and transferred into mammosphere assay medium (DMEM/F-12 media supplemented with 2% B27 (Gibco, 12587010), 20 ng/mL FGF (PeproTech, 100-18B), 20 ng/mL EGF (R&D, 236-EG), 4 μg/mL Heparin, and 0.4% BSA (sigma, A6003-5G)) for long-term culture. To encapsulate single cell in each microgel, HCC1806 cells were suspended in the aforementioned alginate precursor with 16% (v/v) of Optiprep density gradient medium (Sigma). The mammosphere assay medium was refreshed every other day. After cultured for indicated days, the cell viability was determined by Calcein-AM/PI live/dead assay (Beyotime) according to the manufacturer's instructions. The size of spheroids was observed with microscope and measured using ImageJ software.

Live/dead co-staining by Calcein-AM and PI

Spheroids formed in Single-cell-laden microcapsules were washed with PBS three times and then co-stained with a Calcein-AM/PI Cell Viability Assay Kit (Beyotime) with the concentration of Calcein-AM at 2.5 μM and PI 4.5 μM, respectively, at 37℃ for 30 min in the dark. The photographs were captured by an inverted fluorescence microscope, Nikon A1HD25 confocal microscope.

Statistical analysis

Statistical significance between conditions was assessed by Student's t-tests. In all the figures, data are presented as mean ± standard error of the mean (SEM). Significance between conditions is denoted as $^{*}p<0.05$, $^{**}p<0.01$ and $^{***}p<0.001$. At least three independent experiments were performed for each condition for verification of the emphasized trends in in vitro studies.

Supplementary Information

The online version contains supplementary material available at https://doi.org/10.1186/s13072-024-00559-1.

Supplementary Material 1

Supplementary Material 2

Supplementary Material 3

Supplementary Material 4

Supplementary Material 5

Acknowledgements

The authors thank the technical officers at the Department of Biomedical Sciences of City University of Hong Kong for their assistance in using the core facilities; and members of the Chin laboratory for discussions.

Author contributions

Q.H. and J.H. designed the experiments, performed the data collection and analysis, and wrote the manuscript. H.H., T.W., W.L., S.R. and Y.P. designed the experiments, and performed the data collection as well as analysis. L.Z., K.C., M.Y. and X.W. performed data analysis and interpretation. Y.R.C. advised on the experimental design, assisted with manuscript writing and supervised the study.

Funding

This study was supported by General Research Fund (11103719 to Y.R.C) and Research Impact Fund (R1020-18 F to Y.R.C., L.Z., M.Y) from the Research Grants Council (RGC) of the Hong Kong Special Administrative Region, and the City University of Hong Kong (7005739, 7005872, 9609316 to Y.R.C).

Data availability

Data are available upon request. Request for data and reagents shall be directed to Rebecca Chin.

Declarations

Competing interests

The authors declare no competing interests.

Received: 4 June 2024 / Accepted: 3 November 2024
Published online: 10 November 2024

References

1. Sung H, et al. Global Cancer statistics 2020: GLOBOCAN estimates of incidence and Mortality Worldwide for 36 cancers in 185 countries. CA Cancer J Clin. 2021;71(3):209–49.
2. Britt KL, Cuzick J, Phillips KA. Key steps for effective breast cancer prevention. Nat Rev Cancer. 2020;20(8):417–36.
3. Bianchini G, et al. Triple-negative breast cancer: challenges and opportunities of a heterogeneous disease. Nat Rev Clin Oncol. 2016;13(11):674–90.
4. Thandapani P. Super-enhancers in cancer. Pharmacol Ther. 2019;199:129–38.
5. Zhang X, et al. Identification of focally amplified lineage-specific super-enhancers in human epithelial cancers. Nat Genet. 2016;48(2):176–82.
6. Kelly MR, et al. A multi-omic dissection of super-enhancer driven oncogenic gene expression programs in ovarian cancer. Nat Commun. 2022;13(1):4247.
7. Huang H, et al. Defining super-enhancer landscape in triple-negative breast cancer by multiomic profiling. Nat Commun. 2021;12(1):2242.
8. Hu J, et al. TCOF1 upregulation in triple-negative breast cancer promotes stemness and tumour growth and correlates with poor prognosis. Br J Cancer. 2022;126(1):57–71.
9. Bejjani F, et al. The AP-1 transcriptional complex: local switch or remote command? Biochim Biophys Acta Rev Cancer. 2019;1872(1):11–23.
10. Bejjani F, et al. Fra-1 regulates its target genes via binding to remote enhancers without exerting major control on chromatin architecture in triple negative breast cancers. Nucleic Acids Res. 2021;49(5):2488–508.
11. Usui A, et al. The molecular role of Fra-1 and its prognostic significance in human esophageal squamous cell carcinoma. Cancer. 2012;118(13):3387–96.
12. Zhao C, et al. Genome-wide profiling of AP-1-regulated transcription provides insights into the invasiveness of triple-negative breast cancer. Cancer Res. 2014;74(14):3983–94.
13. Sayan AE, et al. Fra-1 controls motility of bladder cancer cells via transcriptional upregulation of the receptor tyrosine kinase AXL. Oncogene. 2012;31(12):1493–503.
14. Chiappetta G, et al. FRA-1 protein overexpression is a feature of hyperplastic and neoplastic breast disorders. BMC Cancer. 2007;7:17.
15. Zhang M, et al. FOSL1 promotes metastasis of head and neck squamous cell carcinoma through super-enhancer-driven transcription program. Mol Ther. 2021;29(8):2583–600.
16. Zhu J, Zhao YP, Zhang YQ. Low expression of FOSL1 is associated with favorable prognosis and sensitivity to radiation/pharmaceutical therapy in lower grade glioma. Neurol Res. 2020;42(6):522–7.
17. Nakajima H, et al. Aberrant expression of Fra-1 in estrogen receptor-negative breast cancers and suppression of their propagation in vivo by ascochlorin, an antibiotic that inhibits cellular activator protein-1 activity. J Antibiot (Tokyo). 2007;60(11):682–9.

18. Franco HL, et al. Enhancer transcription reveals subtype-specific gene expression programs controlling breast cancer pathogenesis. Genome Res. 2018;28(2):159–70.
19. Zajchowski DA, et al. Identification of gene expression profiles that predict the aggressive behavior of breast cancer cells. Cancer Res. 2001;61(13):5168–78.
20. Logullo AF, et al. Role of Fos-related antigen 1 in the progression and prognosis of ductal breast carcinoma. Histopathology. 2011;58(4):617–25.
21. Talotta F, Casalino L, Verde P. The nuclear oncoprotein Fra-1: a transcription factor knocking on therapeutic applications' door. Oncogene. 2020;39(23):4491–506.
22. Casalino L et al. FRA-1 as a Regulator of EMT and metastasis in breast Cancer. Int J Mol Sci, 2023. 24(9).
23. Vallejo A, et al. An integrative approach unveils FOSL1 as an oncogene vulnerability in KRAS-driven lung and pancreatic cancer. Nat Commun. 2017;8:14294.
24. Yao T, et al. Saikosaponin-d alleviates renal inflammation and cell apoptosis in a mouse model of Sepsis via TCF7/FOSL1/Matrix metalloproteinase 9 inhibition. Mol Cell Biol. 2021;41(10):e0033221.
25. Ma L, et al. FOSL1 knockdown ameliorates DSS-induced inflammation and barrier damage in ulcerative colitis via MMP13 downregulation. Exp Ther Med. 2022;24(3):551.
26. Shu S, et al. Response and resistance to BET bromodomain inhibitors in triple-negative breast cancer. Nature. 2016;529(7586):413–7.
27. Hacker G. The morphology of apoptosis. Cell Tissue Res. 2000;301(1):5–17.
28. Rojek KO, et al. Microfluidic Formulation of Topological Hydrogels for Microtissue Engineering. Chem Rev. 2022;122(22):16839–909.
29. Bradner JE, Hnisz D, Young RA. Transcriptional Addict Cancer Cell. 2017;168(4):629–43.
30. Maryam A, Chin YR. ANLN enhances triple-negative breast Cancer Stemness through TWIST1 and BMP2 and promotes its Spheroid Growth. Front Mol Biosci. 2021;8:700973.
31. Lin CI, Yeh NH. Treacle recruits RNA polymerase I complex to the nucleolus that is independent of UBF. Biochem Biophys Res Commun. 2009;386(2):396–401.
32. Werner A, et al. Cell-fate determination by ubiquitin-dependent regulation of translation. Nature. 2015;525(7570):523–7.
33. Mooser C, et al. Treacle controls the nucleolar response to rDNA breaks via TOPBP1 recruitment and ATR activation. Nat Commun. 2020;11(1):123.
34. Shaulian E, Karin M. AP-1 as a regulator of cell life and death. Nat Cell Biol. 2002;4(5):E131–6.
35. Sobolev VV et al. Role of the transcription factor FOSL1 in Organ Development and Tumorigenesis. Int J Mol Sci, 2022. 23(3).
36. Diesch J, et al. Widespread FRA1-dependent control of mesenchymal transdifferentiation programs in colorectal cancer cells. PLoS ONE. 2014;9(3):e88950.
37. Stinson S, et al. miR-221/222 targeting of trichorhinophalangeal 1 (TRPS1) promotes epithelial-to-mesenchymal transition in breast cancer. Sci Signal. 2011;4(186):pt5.
38. Felli N, et al. MicroRNAs 221 and 222 inhibit normal erythropoiesis and erythroleukemic cell growth via kit receptor down-modulation. Proc Natl Acad Sci USA. 2005;102(50):18081–6.
39. Kakumoto K, et al. FRA1 is a determinant for the difference in RAS-induced transformation between human and rat fibroblasts. Proc Natl Acad Sci USA. 2006;103(14):5490–5.
40. Wu J, et al. The Fra-1–miR-134–SDS22 feedback loop amplifies ERK/JNK signaling and reduces chemosensitivity in ovarian cancer cells. Cell Death Dis. 2016;7(9):e2384–2384.
41. Jang MK, et al. The bromodomain protein Brd4 is a positive regulatory component of P-TEFb and stimulates RNA polymerase II-dependent transcription. Mol Cell. 2005;19(4):523–34.
42. Shu S, et al. Synthetic Lethal and Resistance Interactions with BET bromodomain inhibitors in Triple-negative breast Cancer. Mol Cell. 2020;78(6):1096–e11138.
43. Loven J, et al. Selective inhibition of tumor oncogenes by disruption of super-enhancers. Cell. 2013;153(2):320–34.
44. Baker EK, et al. BET inhibitors induce apoptosis through a MYC independent mechanism and synergise with CDK inhibitors to kill osteosarcoma cells. Sci Rep. 2015;5:10120.
45. Zippo A, et al. PIM1-dependent phosphorylation of histone H3 at serine 10 is required for MYC-dependent transcriptional activation and oncogenic transformation. Nat Cell Biol. 2007;9(8):932–44.
46. Dong J, et al. Transcriptional super-enhancers control cancer stemness and metastasis genes in squamous cell carcinoma. Nat Commun. 2021;12(1):3974.
47. Xiong G, et al. FOSL1 promotes tumor growth and invasion in ameloblastoma. Front Oncol. 2022;12:900108.
48. Liu Y, Yue M, Li Z. FOSL1 promotes tumorigenesis in colorectal carcinoma by mediating the FBXL2/Wnt/beta-catenin axis via Smurf1. Pharmacol Res. 2021;165:105405.
49. Milde-Langosch K. The Fos family of transcription factors and their role in tumourigenesis. Eur J Cancer. 2005;41(16):2449–61.
50. Song D, et al. Blocking Fra-1 sensitizes triple-negative breast cancer to PARP inhibitor. Cancer Lett. 2021;506:23–34.
51. Desmet CJ, et al. Identification of a pharmacologically tractable Fra-1/ADORA2B axis promoting breast cancer metastasis. Proc Natl Acad Sci U S A. 2013;110(13):5139–44.
52. Bakiri L, et al. Fra-1/AP-1 induces EMT in mammary epithelial cells by modulating Zeb1/2 and TGFbeta expression. Cell Death Differ. 2015;22(2):336–50.

Publisher's note